

# Quantum Measurement-induced Dynamics of Many-Body Ultracold Bosonic and Fermionic Systems in Optical Lattices

Gabriel Mazzucchi,\* Wojciech Kozłowski,† Santiago F. Caballero-Benitez, Thomas J. Elliott, and Igor B. Mekhov  
*Department of Physics, Clarendon Laboratory, University of Oxford,  
Parks Road, Oxford OX1 3PU, United Kingdom*

(Dated: June 19, 2022)

Trapping ultracold atoms in optical lattices enabled numerous breakthroughs uniting several disciplines. Although the light is a key ingredient in such systems, its quantum properties are typically neglected, reducing the role of light to a classical tool for atom manipulation. Here we show how elevating light to the quantum level leads to novel phenomena, inaccessible in setups based on classical optics. Interfacing a many-body atomic system with quantum light opens it to the environment in an essentially nonlocal way, where spatial coupling can be carefully designed. The competition between typical processes in strongly correlated systems (local tunnelling and interaction) with global measurement backaction leads to novel multimode dynamics and the appearance of long-range correlated tunnelling capable of entangling distant lattice sites, even when tunnelling between neighbouring sites is suppressed by the quantum Zeno effect. We demonstrate both the break-up and protection of strongly interacting fermion pairs by different measurements.

Ultracold gases trapped in optical lattices represent a successful interdisciplinary field: Atomic systems allow quantum simulations of phenomena predicted in condensed matter and particle physics, and find applications in quantum information processing [1]. Although light plays a key role in such systems, its quantum properties have been neglected in most works, reducing it to a classical tool for creating intriguing atomic states. Here, we introduce the quantumness of light into strongly correlated atomic systems and demonstrate phenomena that cannot be realised using classical optical setups. The recognized advantage of ultracold gases in contrast to condensed matter materials is their isolation from the environment. However, this creates a challenge to introduce any controlled dissipation (e.g. atom losses and collisions are difficult to manipulate). Here we show that coupling atoms to quantized light, which can be continuously measured, introduces a controllable decoherence channel into

many-body dynamics. Moreover, global light scattering from multiple lattice sites creates nontrivial, spatially nonlocal coupling to the environment, which is impossible to obtain with local interactions [2]. Such a quantum optical approach can broaden the field even further, allowing quantum simulation of models unobtainable using classical light, and the design of novel systems beyond condensed matter analogues.

Collapse of the atomic wave function, when only the scattered light is measured, reflects the measurement backaction. This is one of the most fundamental manifestations of quantum mechanics [3], here due to the light-matter entanglement. We demonstrate how this backaction and the spatially nonlocal quantum Zeno effect, being introduced in a strongly correlated system, compete with many-body dynamics defined by standard local processes (tunnelling and on-site interaction). Highlighting such competition takes one beyond recent quantum non-demolition (QND) approaches [4–10], where either many-body dynamics or measurement backaction did not play any role. For bosons, it leads to the emergence of dynamical macroscopic superpositions (multimode Schrödinger cat states). For strongly interacting fermions, we demonstrate the measurement-induced break-up and protection of fermion pairs. Even if standard tunnelling between neighbouring sites is suppressed by the quantum Zeno effect, long-range correlated tunnelling appears, leading to dynamical generation entanglement between distant sites. The generated spatial modes of matter fields can be considered as designed systems and reservoirs. We can make analogy with famous cavity QED experiments [3], where the quantum light states in a cavity were probed and projected by measuring atoms. Here, light and matter are reversed and we probe matter-fields with light. A striking advancement is that the number of quantum matter waves (sites with trapped atoms) can be easily scaled from few to thousands by changing the number of illuminated sites, while scaling cavities is an extreme challenge [3]. This work, together with recent experi-

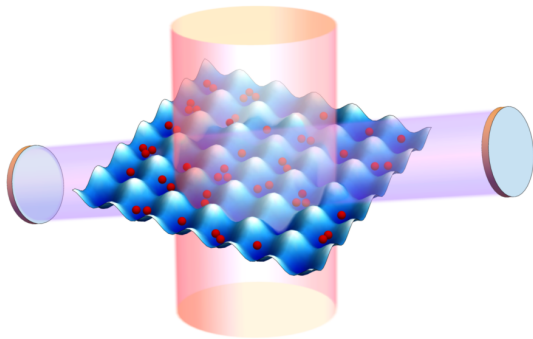


Figure 1. **Setup.** Atoms in an optical lattice are probed by a coherent light beam, and the light scattered at a particular angle is enhanced and collected by a leaky cavity.

\* gabriel.mazzucchi@physics.ox.ac.uk

† wojciech.kozlowski@physics.ox.ac.uk

ments where our predictions can be tested (Bose-Einstein Condensates trapped inside a cavity [11–13]), will help to close the gap between quantum optics and quantum gases, by joining quantized light and strongly correlated many-body systems, thus approaching the fully quantum regime of light-matter interaction [5, 14, 15].

We consider off-resonant light scattering from  $N$  atoms trapped in an optical lattice with period  $d$  and  $L$  sites [14] (see Methods and Fig. 1). The light scattered at a particular angle can be selected and enhanced by a cavity [16] with decay rate  $\kappa$ . Similar to classical optics, the light amplitude is given by a sum of scatterings from all atoms with coefficients dependent on their positions:  $a = C(\hat{D} + \hat{B})$ , where  $a$  is the photon annihilation operator,  $C$  is the Rayleigh scattering coefficient and

$$\hat{D} = \sum_{j=1}^L J_{jj} \hat{n}_j, \quad \hat{B} = \sum_{\langle i,j \rangle} J_{ij} b_i^\dagger b_j, \quad (1)$$

where  $b_j$  and  $\hat{n}_j = b_j^\dagger b_j$  are the atomic annihilation and number operators at site  $j$  ( $\langle i, j \rangle$  sums over neighbouring sites), and  $J_{ij}$  are given in Methods. In equation (1)  $\hat{D}$  describes scattering from the on-site densities, while  $\hat{B}$  that from the small inter-site densities [17]. For well-localised atoms, the second term is usually neglected, and  $a = C\hat{D}$  with  $J_{jj} = u_{\text{out}}^*(\mathbf{r}_j)u_{\text{in}}(\mathbf{r}_j)$ , where  $u(\mathbf{r})$  are the mode functions of input and scattered light (e.g.,  $u_{\text{in,out}}(\mathbf{r}) = \exp(i\mathbf{k}_{\text{in,out}} \cdot \mathbf{r})$  for travelling and  $u_{\text{in,out}}(\mathbf{r}) = \cos(\mathbf{k}_{\text{in,out}} \cdot \mathbf{r})$  for standing waves with wave vectors  $\mathbf{k}_{\text{in,out}}$ ). (A peculiar case of light scattering from inter-site regions [17], where  $a = C\hat{B}$ , will be underlined here later). For spin- $\frac{1}{2}$  fermions we use two light polarizations  $a_{x,y}$  that couple differently to two spin densities  $\hat{n}_{\uparrow j}, \hat{n}_{\downarrow j}$  allowing measurement of their linear combinations, e.g.,  $a_x = C\hat{D}_x = C\sum_{j=1}^L J_{jj} \hat{\rho}_j$  and  $a_y = C\hat{D}_y = C\sum_{j=1}^L J_{jj} \hat{m}_j$ , where  $\hat{\rho}_j = \hat{n}_{\uparrow j} + \hat{n}_{\downarrow j}$  and  $\hat{m}_j = \hat{n}_{\uparrow j} - \hat{n}_{\downarrow j}$  are the mean density and magnetisation. This property has recently been used to investigate spin-spin correlations in Fermi gases [18, 19].

We focus on a single run of a continuous measurement experiment using the quantum trajectories technique [20] (see Methods). The evolution is determined by a stochastic process described by quantum jumps (the jump operator  $c = \sqrt{2\kappa}a$  is applied to the state when a photodetection occurs) and non-Hermitian evolution with the Hamiltonian  $\hat{H}_{\text{eff}} = \hat{H}_0 - i\hbar c^\dagger c/2$  between jumps, where  $H_0$  is the usual (Bose-)Hubbard Hamiltonian. Importantly, the measurement introduces a new energy and time scale  $\gamma = |C|^2\kappa$ , which competes with the two other standard scales responsible for unitary dynamics of closed systems (tunnelling  $J$  and on-site interaction  $U$ ). If atoms scatter light independently in uncontrolled directions (as in spontaneous emission [21] or local addressing), independent jump operators  $c_j$  would be applied to each site, projecting the atomic state to a fully mixed state [21]. In contrast, here we consider global

coherent scattering, where the single global jump operator  $c$  is given by the sum over all sites, and the local coefficients  $J_{jj}$  (1) responsible for the atom-environment coupling (via the light mode  $a$ ) can be engineered by optical geometry. Thus, atoms are coupled to the environment globally, and atoms that scatter light with the same phase are indistinguishable to light scattering (i.e. there is no “which-path information”). As a striking consequence, the quantum superpositions are strongly preserved in the final projected states, and the systems splits into several spatial modes [22], where all atoms belonging to the same mode are indistinguishable, while being distinguishable from atoms belonging to different modes.

We engineer the atom-environment coupling coefficients  $J_{jj}$  using standing or traveling waves at different angles to the lattice. If both probe and scattered light are standing waves crossed at such angles to the lattice that projection  $\mathbf{k}_{\text{in}} \cdot \mathbf{r}$  is equal to  $\mathbf{k}_{\text{out}} \cdot \mathbf{r}$  and shifted such that all even sites are positioned at the nodes (do not scatter light), one gets  $J_{jj} = 1$  for odd and  $J_{jj} = 0$  for even sites. Thus we measure the number of atoms at odd sites only (the jump operator is proportional to  $\hat{N}_{\text{odd}}$ ), introducing two modes, which scatter light differently: odd and even sites. The coefficients  $J_{jj} = (-1)^j$  are designed by crossing light waves at  $90^\circ$  such that atoms at neighboring sites scatter light with  $\pi$  phase difference [4, 10, 23–25], giving  $\hat{D} = \hat{N}_{\text{even}} - \hat{N}_{\text{odd}}$ , introducing the same modes, but with different coherence between them. Moreover, using travelling waves crossed at the angle such that each  $R$ -th site is indistinguishable ( $(\mathbf{k}_{\text{in}} - \mathbf{k}_{\text{out}}) \cdot \mathbf{r}_j = 2\pi j/R$ ), introduces  $R$  modes with macroscopic atom numbers  $\hat{N}_l$ :  $\hat{D} = \sum_{l=1}^R \hat{N}_l e^{i2\pi l/R}$ . Here two (odd- and even-site modes) appear for  $R = 2$ . Therefore, we reduce the jump (measurement) operator from being a sum of numerous microscopic contributions from individual sites to the sum of smaller number of macroscopically occupied modes with a very nontrivial spatial overlap between them. In the following, we will show how such globally designed measurement backaction introduces spatially long-range interactions of these modes, and demonstrate novel effects resulting from the competition of mode dynamics with standard local processes in a many-body system.

We start with non-interacting bosons ( $U/J = 0$ ), and demonstrate the competition between global measurement and local tunnelling. Because of such competition, the weak measurement ( $\gamma \ll J$ ) is unable to freeze the atom numbers as expected for quantum Zeno dynamics [26–28]. In contrast, atom-number measurement leads to giant oscillations of particle number between the modes. In Figs. 2a-c we show the atom number distributions in one of the modes for  $R = 2$  ( $N_{\text{odd}}$ ) and  $R = 3$  ( $N_1$ ). Without measurement, these distributions would spread strongly and may show only oscillation amplitudes proportional to the initially created imbalance (thus, tiny oscillations for initially tiny imbalance). In contrast, here we observe (i) full exchange of atoms between the modes independent of the initial state, (ii) the distributions con-

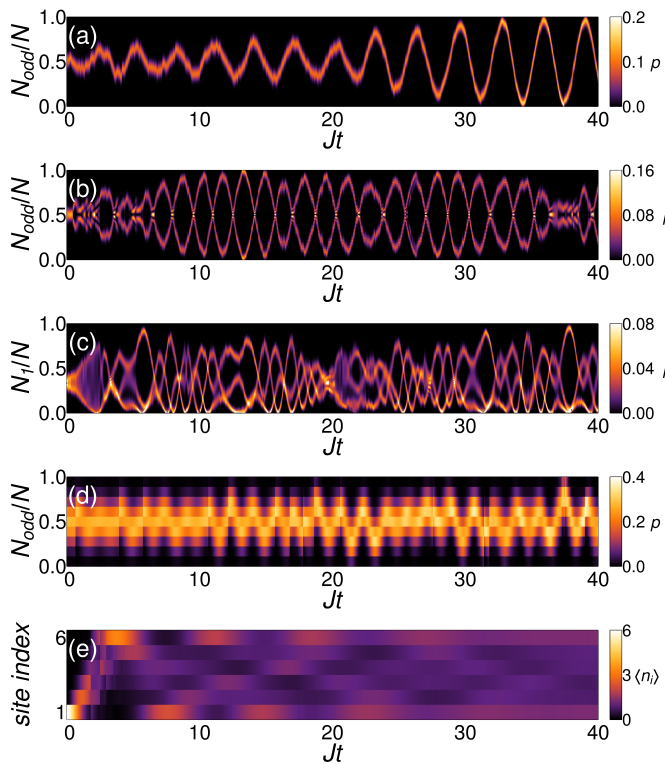


**Figure 2. Large oscillations between the measurement-induced spatial modes resulting from the competition between tunnelling and weak-measurement backaction.** The plots show single quantum trajectories. **a-d**, Atom number distributions  $p(N_i)$  in one of the modes, which show various number of well-squeezed components, reflecting the creation of macroscopic superposition states depending on the measurement configuration ( $U/J = 0$ ,  $\gamma/J = 0.01$ ,  $L = N$ , initial states: superfluid for bosons, Fermi sea for fermions). **a**, Measurement of the atom number at odd sites  $\hat{N}_{\text{odd}}$  creates one strongly oscillating component in  $p(N_{\text{odd}})$  ( $N = 100$  bosons). **b**, Measurement of  $(\hat{N}_{\text{odd}} - \hat{N}_{\text{even}})^2$  introduces  $R = 2$  modes and preserves the superposition of positive and negative atom number differences in  $p(N_{\text{odd}})$  ( $N = 100$  bosons). **c**, Measurement for  $R = 3$  modes (see text) preserves 3 components in  $p(N_1)$  ( $N = 108$  bosons). **d**, Measurement of  $\hat{N}_{\text{odd}}$  for fermions leads to oscillations in  $p(N_{\text{odd}})$ , though not as well squeezed as for bosons because of Pauli blocking ( $L = 8$  sites,  $N_{\uparrow} = N_{\downarrow} = 4$  fermions). **e**, On-site atom numbers  $\langle \hat{n}_i \rangle$  for measurement of the matter-field coherence between the sites  $\hat{B}$ . Atoms, all initially at the edge site, are quickly spread across the whole lattice leading to the large uncertainty in the atom number, while the matter-phase related variable is defined (projected) by the measurement (bosons,  $N = L = 6$ ,  $U/J = 0$ ,  $\gamma/J = 0.1$ ). Simulations for 1D lattice.

sist of a small number of well-defined components, and (iii) these components are squeezed even by weak measurement. The multi-component structure is explained by the degeneracy of spatially multimode states, as the measurement of photon number (intensity)  $a^\dagger a$  is not sensitive to the light phase. Therefore, all permutations of

mode occupations that scatter light with the same intensity are indistinguishable. For  $R = 2$ , the state is 2-fold degenerate, for  $R > 2$  it is  $2R$ -fold degenerate. Fig. 2b reflects the superposition of two states with positive and negative  $N_{\text{odd}} - N_{\text{even}}$ , while Fig. 2c reflects the superposition in the three-mode case. As an important consequence, one gets a dynamical method to prepare multi-component macroscopic superpositions (Schrödinger cat or NOON states), which are useful in quantum metrology and information. This method is deterministic without need for external quantum control [29, 30], as the continuously monitored intensity directly shows, when the number splitting in the components reaches its maximum (corresponding to the maximal macroscopicity [31]), and the lattice depth can be ramped up to freeze further dynamics. Such states are indeed fragile to decoherence such as photon losses, but setups can be modified to make them more robust [32]. In addition, the state in Fig. 2a consists of only one component (here  $N_{\text{odd}}$  is measured directly) and is therefore insensitive to photon losses. Reducing the number of modes and components can enable study the transition between quantumness and classicality, where nontrivial superpositions cannot exist [33].

We found that for many atoms, the  $R$ -mode problem can be treated analytically reducing it to  $R$  sites, if the initial state is superfluid. Giant oscillations are explained by the action of an effective quasi-periodic driving force due to the measurement backaction. In particular, for  $R = 2$  (effective double-well [34, 35]), we showed that the system leaves its stationary state ( $N_{\text{odd}} = N_{\text{even}}$ ) with the increment  $N\gamma/2$ . Note that dynamics described here will be visible already in a single experimental run. In contrast, averaging over many runs, which corresponds to the master equation solution, masks such effects completely. This happens because the oscillation phase changes from realization to realization as is known from works involving single and multiple measurements [36].

In contrast to bosons, dynamics for two modes of non-interacting fermions does not show well-defined oscillations (Fig. 2d) due to Pauli exclusion. However, while the initial ground state is a product of  $\uparrow$  and  $\downarrow$  wave functions (Slater determinants), the measurement introduces an effective interaction between two spin components and the state gets entangled by measurement.

Carefully choosing geometry, one can suppress the on-site contribution to light scattering and effectively concentrate light between the sites, thus in-situ measuring the matter-field interference  $b_i^\dagger b_{i+1}$  [17]. In this case,  $a = C\hat{B}$ , and the coefficients  $J_{ij}$  (1) can be engineered [17]. For  $J_{ij} = 1$ , the jump operator is proportional to the kinetic energy  $E_K$  and tends to freeze the system in eigenstates of the non-interacting Hamiltonian. Being insensitive to the sign of  $E_K$ , the measurement projects to a superposition of states with opposite kinetic energies: a superposition of matter waves propagating with different momenta. The measurement freezes dynamics for any  $\gamma/J$ , since the jump operator and  $\hat{H}_{\text{eff}}$  have the

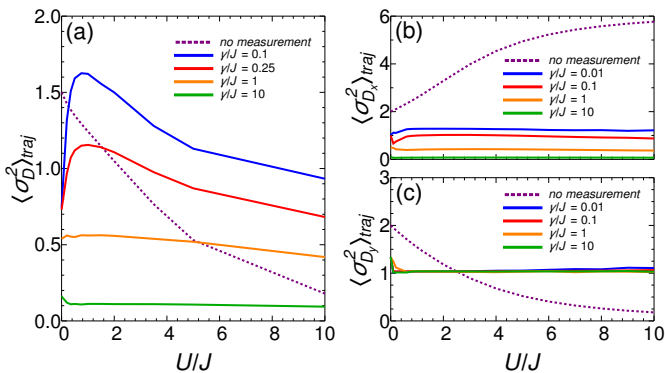


**Figure 3. Atom number fluctuations demonstrating the competition of global measurement with local interaction and tunnelling.** Number variances are averaged over many trajectories. **a**, Bose-Hubbard model with repulsive interaction. The fluctuations of the atom number at odd sites  $\hat{N}_{\text{odd}}$  in the ground state without a measurement (dashed line) decrease as  $U/J$  increases, reflecting the transition between superfluid and Mott insulator phases. For the weak measurement,  $\langle \sigma_D^2 \rangle_{\text{traj}}$  is squeezed below the ground state value, but then increases and reaches its maximum as the atom repulsion prevents oscillations and makes the squeezing less effective. In the strong interacting limit, the Mott insulator state is destroyed and the fluctuations are larger than in the ground state. (100 trajectories,  $N = L = 6$ .) **b,c**, Fermionic Hubbard model with attractive interaction; fluctuations of the total atom number at odd sites  $\hat{D}_x = \hat{N}_{\uparrow\text{odd}} + \hat{N}_{\downarrow\text{odd}}$  (**b**) and of the magnetisation at odd sites  $\hat{D}_y = \hat{M}_{\text{odd}} = \hat{N}_{\uparrow\text{odd}} - \hat{N}_{\downarrow\text{odd}}$  (**c**). Without measurement, the interaction favours formation of doubly occupied sites so the density fluctuations in the ground state are increasing while the magnetisation ones are decreasing. The measurement creates singly occupied sites decreasing the density fluctuations and increasing the magnetisation ones, which manifests the break-up of fermion pairs by measurement. The measurement-based protection of fermion pairs is shown in the next figure. (100 trajectories,  $L = 8$ ,  $N_{\uparrow} = N_{\downarrow} = 4$ .) Simulations for 1D lattice.

same eigenstates. As a result of the detection, the atoms quickly spread across the lattice, and the density distribution becomes uncertain (Fig. 2e), clearly illustrating the quantum uncertainty relation between the number- and phase-related variables ( $\hat{n}_i$  and  $b_i^\dagger b_{i+1}$ ). Engineering  $J_{ij}$ , can lead to the measurement-based preparation of peculiar multicomponent momentum (or Bloch) states.

Including the interactions ( $U/J \neq 0$ ), dynamics changes as the measurement competes with both tunnelling and interaction. To highlight this, we focus on the variance of the measured variable averaged over many trajectories  $\langle \sigma_D^2 \rangle_{\text{traj}}$ , when it reaches its steady state. In Fig. 3, we show results for the measurement of  $\hat{N}_{\text{odd}}$ .

For bosons (Fig. 3a), without measurement the number fluctuations  $\sigma_D^2$  monotonically decrease for increasing  $U$ , reflecting the superfluid - Mott insulator phase transition. However, the measurement changes this behaviour and  $\langle \sigma_D^2 \rangle_{\text{traj}}$  varies non-monotonically. For weak interac-

tion, the fluctuations are strongly squeezed below those of the ground state; they then quickly increase, reach their maximum, and subsequently decrease as the interaction becomes stronger. We explain this effect by looking at single trajectories: For small  $U/J$ , as described above, the measurement strongly squeezes the occupation of one mode (Fig. 2a). However, the local atom repulsion prevents the formation of states with high population in one of two modes (Fig. 4a). Because of the local interaction, states with different imbalances oscillate with different frequencies and, hence, the measurement does not decrease the fluctuations of  $\hat{N}_{\text{odd}}$  as efficiently as in the non-interacting case. For large  $U$ , both global measurement and local interaction tend to squeeze the fluctuations, but as the measurement destroys the Mott insulator, the fluctuations are larger than in the ground state.

For fermions (Figs. 3b,c), the ground state of the attractive Hubbard model in the strong interacting regime contains mainly doubly occupied sites (pairs). Therefore, without measurement, the fluctuations of total population  $\hat{D}_x = \hat{N}_{\uparrow\text{odd}} + \hat{N}_{\downarrow\text{odd}}$  ( $\sigma_{D_x}^2$ ) increase with  $U/J$  as empty or doubly occupied sites become more probable. We can probe either the total population  $\hat{D}_x$ , or both total population and magnetisation  $\hat{D}_y = \hat{M}_{\text{odd}} = \hat{N}_{\uparrow\text{odd}} - \hat{N}_{\downarrow\text{odd}}$ . In the first case (Figs. 3b,c), the measurement quickly squeezes  $\sigma_{D_x}^2$ , but destroys the pairs as it does not distinguish between singly or doubly occupied sites. This manifests the break-up of local fermion pairs by the global measurement and the corresponding trajectory is shown in Figs. 4c: while initially dynamics contains only even values of  $\hat{N}_{\text{odd}}$  (i.e. pairs), the measurement also creates unpaired (odd) fermion numbers. In contrast, measuring both density and magnetisation reduces their fluctuations (i. e. unpaired fermions) and increases the lifetime of doubly occupied sites. This manifests the measurement-induced protection of fermion pairs and the trajectory is shown in Fig. 4d: The number distribution contains only even values of  $N_{\text{odd}}$  indicating that fermions tunnel only in pairs.

When the measurement is strong ( $\gamma \gg J$ ), we will show the following nontrivial spatial effects. First, the measurement can freeze the mode atom numbers, thus decorrelating the numbers in different modes, while protecting typical dynamics within each mode. Second, even if the modes are number-decorrelated and the standard tunnelling between them is suppressed by the quantum Zeno effect (i.e. close to full projection), they can still be entangled by another process. We show that higher-order long-range correlated multi-tunnelling events appear: e.g., atoms can tunnel only in pairs (second order tunnelling) and, importantly, this pair is delocalized and correlated in space. Although for clarity we demonstrate such phenomena in Fig. 5 for small systems, they also hold for macroscopic modes.

First (Fig. 5a), we freeze the atom number  $\hat{N}_{\text{illum}}$  in the central illuminated region by detecting light in the diffraction maximum ( $a = C\hat{N}_{\text{illum}}$ ) [10, 32]. The lattice

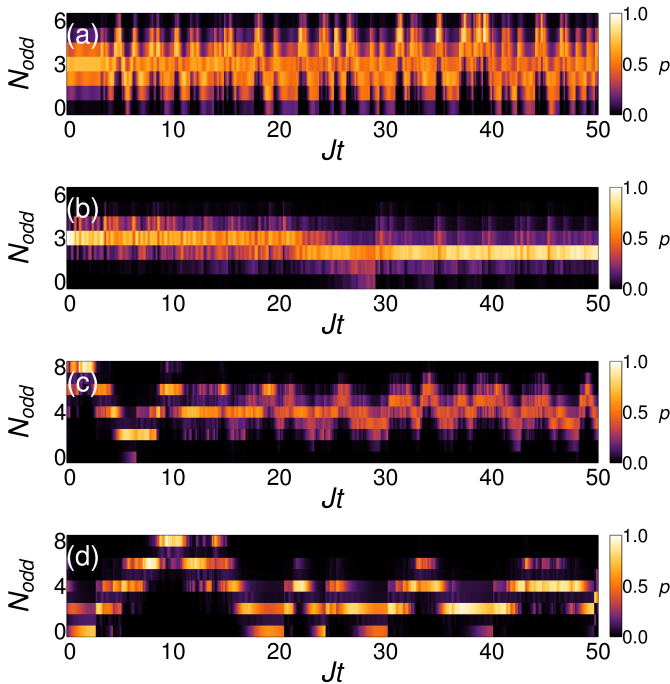


Figure 4. **Conditional dynamics of the atom-number distributions at odd sites illustrating competition of the global measurement with local interaction and tunnelling.** Single quantum trajectories, initial states are the ground states. **a**, Weakly interacting bosons: the on-site repulsion prevents the formation of well-defined oscillations in the population of the mode. As states with different imbalance evolve with different frequencies, the squeezing due to the measurement is not as efficient as one observed in the non-interacting case ( $N = L = 6$ ,  $U/J = 1$ ,  $\gamma/J = 0.1$ ). **b**, Strongly interacting bosons: oscillations are completely suppressed and the number of atoms in the mode is rather well-defined, although is less squeezed as in the Mott insulator. ( $N = L = 6$ ,  $U/J = 10$ ,  $\gamma/J = 0.1$ ). **c**, Attractive fermionic Hubbard model in the strong interaction limit. Measuring only the total population at odd sites  $\hat{D}_x = \hat{N}_{\uparrow\text{odd}} + \hat{N}_{\downarrow\text{odd}}$  quickly creates singly occupied sites, demonstrating measurement-induced break-up of fermion pairs ( $L = 8$ ,  $N_{\uparrow} = N_{\downarrow} = 4$ ,  $U/J = 10$ ,  $\gamma/J = 0.1$ ). **d**, The same as **c**, but with added measurement of the magnetisation at odd sites  $\hat{D}_y = \hat{M}_{\text{odd}} = \hat{N}_{\uparrow\text{odd}} - \hat{N}_{\downarrow\text{odd}}$ . This protects the doubly occupied sites, thus, demonstrating protection of fermion pairs by measurement. The distribution of  $N_{\text{odd}}$  vanishes for odd numbers, implying that the fermions tunnel only in pairs. Simulations for 1D lattice.

is thus divided into two modes: non-illuminated zones 1 and 3 and the illuminated one 2 (Fig. 5a.1). Typical dynamics occurs within each zone, but the standard tunnelling between the zones is suppressed (Fig. 5a.2). Importantly, atoms can still penetrate, if the process does not change  $N_{\text{illum}}$ : An atom from 1 can tunnel to 2, if simultaneously one atom tunnels from 2 to 3. Thus, effective long-range tunnelling between two spa-

tially disconnected zones 1 and 3 happens due to two-step processes  $1 \rightarrow 2 \rightarrow 3$  or  $3 \rightarrow 2 \rightarrow 1$ . This is supported by the negative (anti-)correlations  $\langle \delta N_1 \delta N_3 \rangle = \langle N_1 N_3 \rangle - \langle N_1 \rangle \langle N_3 \rangle$  showing that an atom disappearing in 1 appears in 3, while there are no correlations between illuminated and non-illuminated regions,  $\langle (\delta N_1 + \delta N_3) \delta N_2 \rangle = 0$  (Fig. 5a.4). Surprisingly, the correlated tunnelling still builds entanglement between illuminated and non-illuminated regions (Fig. 5a.3) underlying the intermediate (virtual) step in the two-tunnelling event. This effect may lead to creation of intriguing multipartite entangled states with no simple classical correlations [37].

To make correlated tunnelling visible even in the mean atom number, we consider illumination of all even sites (Fig. 5b) thus freezing both  $N_{\text{even}}$  and  $N_{\text{odd}}$ . Fig. 5b.2 shows that while  $N_{\text{even}}$  is fixed, there is a slow atom exchange between odd sites, although they are disconnected. Fig. 5b.1 clarifies the nontrivial character of correlated tunnelling. The correlations can appear between all possible tunnellings leading to the fixed atom numbers of modes. This again suggests that global coherent addressing favours correlated tunnelling, in contrast to local uncorrelated addressing of individual sites that should decrease the probability of individual tunnelling events being correlated. Scheme in Fig. 5b.1 can help to design a nonlocal reservoir for the tunnelling (or decay) of atoms from one region to another. For example, if the atoms are placed only at odd sites, their standard tunnelling is strongly suppressed as there is no second tunnelling event. If, however, one adds some atoms to even sites (even if they are far from the initial atoms), the slow correlated tunnelling ("decay") becomes allowed and its rate can be tuned by the number of added atoms. This resembles the repulsively bound pairs created by local interactions [38]. In contrast, here the atoms are long-range correlated due to the global measurement.

The negative number correlations are typical for systems with constraints (superselection rules) such as fixed atom number. The constraints implied by our global measurement are more general. For example, in Fig. 5c we show the generation of positive number correlations (shown in Fig. 5c.4) by freezing the atom number difference between the sites ( $N_{\text{odd}} - N_{\text{even}}$ , by measuring at the diffraction minimum). Thus, atoms can only enter or leave this region in pairs, which again is possible due to correlated tunnelling (Figs. 5c1-2) and manifests positive correlations. Note that, using more modes, the design of higher-order multi-tunnelling events is possible.

In summary, we introduced global quantum measurement in strongly correlated many-body systems and demonstrated the competition between the global back-action and standard local processes. It leads to spatially multimode dynamics producing macroscopic superpositions useful for quantum information and metrology. We showed the possibility of measurement-induced break-up and protection of strongly interacting fermion pairs. For strong measurement, when the quantum Zeno ef-

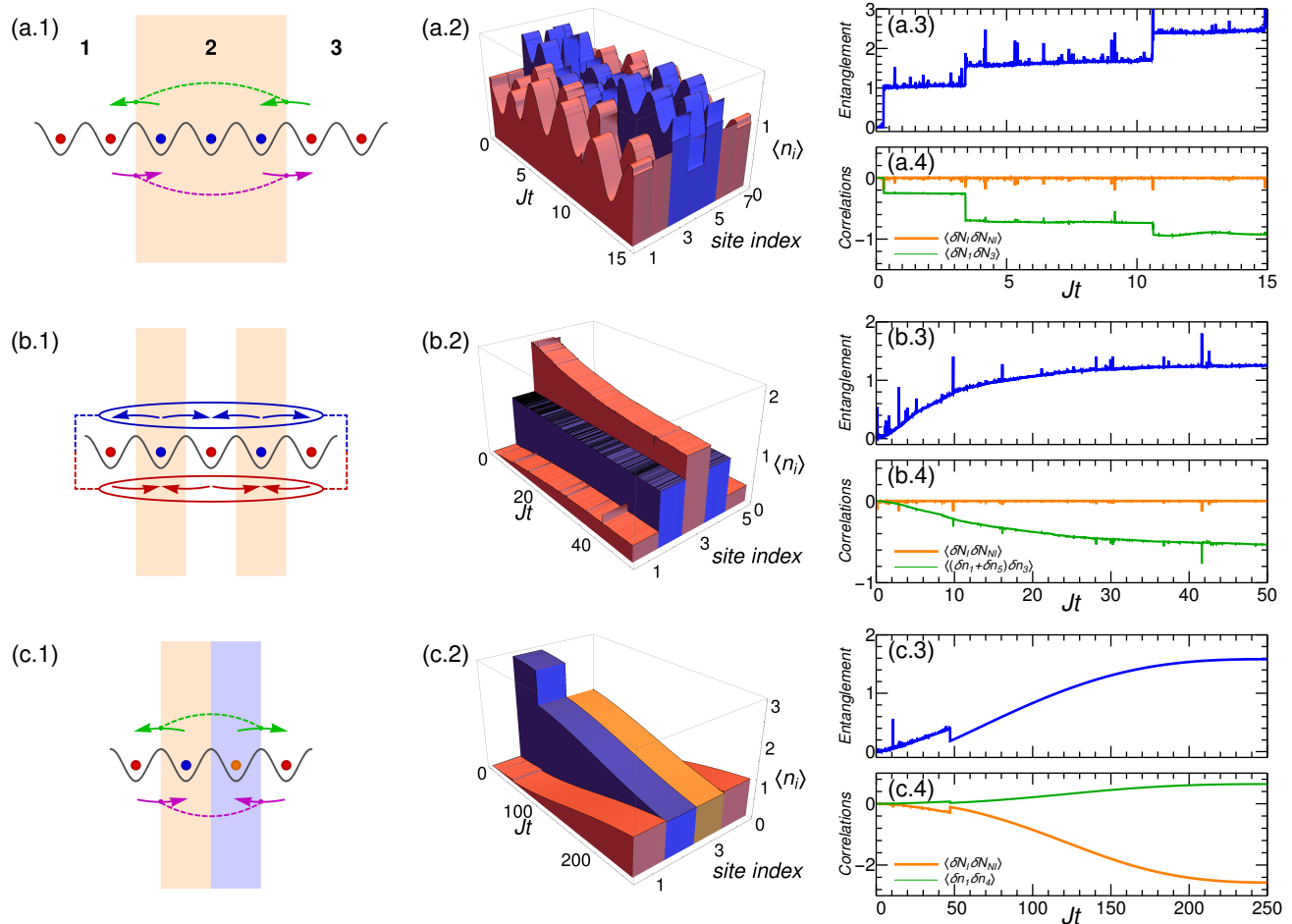


Figure 5. **Long-range correlated tunnelling and entanglement, dynamically induced by strong global measurement.** **a,b,c** show different measurement geometries, implying different constraints. Panels (1): schematics of long-range tunnellings, when standard short-range ones are Zeno-suppressed. Panels (2): evolution of on-site densities; atoms effectively tunnel between disconnected regions due to correlations. Panels (3): entanglement entropy growth between illuminated and non-illuminated regions. Panels (4): correlations between different modes (orange) and within the same mode (green); atom number  $N_I$  ( $N_{NI}$ ) in illuminated (non-illuminated) mode. **a**, Atom number in the central region is frozen: system is divided into three regions and correlated tunnelling occurs between non-illuminated zones (a.1). Standard dynamics happens within each region, but not between them (a.2). Entanglement build up (a.3). Negative correlations between non-illuminated regions (green) and zero correlations between two modes (orange) (a.4). Initial state:  $|1, 1, 1, 1, 1, 1, 1\rangle$ ,  $\gamma/J = 100$ . **b**, Even sites are illuminated, freezing  $N_{\text{even}}$  and  $N_{\text{odd}}$ . Long-range tunnelling is represented by any pair of blue and red arrows (b.1). Correlated tunnelling occurs between non-neighbouring sites without changing mode populations (b.2). Entanglement build up (b.3). Negative correlations between edge sites (green) and zero correlations between two modes (orange) (b.4). Initial state:  $|0, 1, 2, 1, 0\rangle$ ,  $\gamma/J = 100$ . **c**, Atom number difference between two central sites is frozen. Correlated tunnelling leads to exchange of long-range atom pairs between illuminated and non-illuminated regions (c.1,2). Entanglement build up (c.3). In contrast to previous examples, sites in the same zones (illuminated/ non-illuminated) are positively correlated (green), while atoms in different zones are negatively correlated (orange) (c.4). Initial state:  $|0, 3, 1, 0\rangle$ ,  $\gamma/J = 500$ . 1D lattice,  $U/J = 0$ .

fect suppresses usual short-range tunnelling, the atoms can still effectively tunnel even to distant sites due to the long-range correlated tunnelling induced by global measurement. Moreover, such a nonlocal high-order tunnelling creates entanglement between zones disconnected by the measurement, which is not visible in density-density correlations. Quantum optical engineering of

nonlocal coupling to environment, combined with quantum measurement, can allow the design of nontrivial system-bath interactions, enabling new links to quantum simulations [39] and thermodynamics [40]. Our predictions can be tested using both macroscopic measurements [11–13, 41] as well as novel methods based on single-site resolution [42–45]. Based on off-resonant scat-

tering and thus being non-sensitive to a detailed level structure, our approach can be applied to other arrays of natural or artificial quantum objects: molecules [46], ions [47], atoms in multiple cavities [48], semiconductor [49] or superconducting [50] qubits.

## ACKNOWLEDGMENTS

The work was supported by the EPSRC (DTA and EP/I004394/1).

## METHODS

We describe atomic dynamics by the (Bose-) Hubbard Hamiltonian. For the bosonic case,

$$\hat{H}_0 = -\hbar J \sum_{\langle i,j \rangle} b_j^\dagger b_i + \hbar \frac{U}{2} \sum_i \hat{n}_i (\hat{n}_i - 1), \quad (2)$$

while for the fermionic case

$$\hat{H}_0 = -\hbar J \sum_{\sigma=\uparrow,\downarrow} \sum_{\langle i,j \rangle} f_{j,\sigma}^\dagger f_{i,\sigma} - \hbar U \sum_i \hat{n}_{i,\uparrow} \hat{n}_{i,\downarrow}, \quad (3)$$

where  $b$  and  $f_\sigma$  are respectively the bosonic and fermionic annihilation operators,  $\hat{n}$  is the atom number operator,  $U$  and  $J$  are the on-site interaction and tunnelling coefficients. The Hamiltonian of the light-matter system is [14]

$$\hat{H} = \hat{H}_0 + \sum_l \hbar \omega_l a_l^\dagger a_l + \hbar \sum_{l,m} U_{lm} a_l^\dagger a_m \hat{F}_{lm} \quad (4)$$

where  $a_l$  are the photon annihilation operators for the light modes with frequencies  $\omega_l$ ,  $U_{lm} = g_l g_m / \Delta_a$ ,  $g_l$  are the atom-light coupling constants, and  $\Delta_a = \omega_p - \omega_a$  is the probe-atom detuning. The operator  $\hat{F}_{lm} = \hat{D}_{lm} + \hat{B}_{lm}$  couples atomic operators to the light fields:

$$\hat{D}_{lm} = \sum_i J_{ii}^{lm} \hat{n}_i, \quad \hat{B}_{lm} = \sum_{\langle i,j \rangle} J_{ij}^{lm} b_i^\dagger b_j, \quad (5)$$

$$J_{ij}^{lm} = \int w(\mathbf{r} - \mathbf{r}_i) u_l^*(\mathbf{r}) u_m(\mathbf{r}) w(\mathbf{r} - \mathbf{r}_j) d\mathbf{r}. \quad (6)$$

$\hat{F}_{lm}$  originations from the overlaps between the light mode functions  $u_l(\mathbf{r})$  and density operator  $\hat{n}(\mathbf{r}) =$

$\hat{\Psi}^\dagger(\mathbf{r})\hat{\Psi}(\mathbf{r})$ , after the matter-field operator is expressed via Wannier functions:  $\hat{\Psi}(\mathbf{r}) = \sum_i b_i w(\mathbf{r} - \mathbf{r}_i)$ .  $\hat{D}_{lm}$  sums the density contributions  $\hat{n}_i$ , while  $\hat{B}_{lm}$  sums the matter-field interference terms. The light-atom coupling via operators assures the dependence of light on the atomic quantum state. These equations can be extended to fermionic atoms introducing an additional index for the polarisation of light modes.

From (3) we can compute the Heisenberg equation for light operators in the stationary limit [14]. Specifically, we consider two light modes: a coherent probe beam  $a_0$  and the scattered light  $a_1$ , which is enhanced by a cavity with the decay rate  $\kappa$ . This allows us to express  $a_1$  as

$$a_1 = \frac{iU_{10}a_0}{i\Delta_p - \kappa} \hat{F}_{10} \equiv C \hat{F}_{10} \quad (7)$$

where  $\Delta_p = \omega_0 - \omega_1$  is the probe-cavity detuning, and  $C$  is the cavity analogue of the Rayleigh scattering coefficient in free space [17]. In the main text, we drop the subscript in  $a_1$  and superscripts in  $J_{ij}^{lm}$ .

Quantum trajectories describe the evolution of a quantum system conditioned on the result of a measurement [20]. It is possible to represent dynamics of a system with two different processes: non-Hermitian dynamics and quantum jumps. The first one describes evolution of the system between two consecutive measurement events, while the second one models the photodetections. These can be simulated introducing the jump operator  $c = \sqrt{2\kappa}a_1$  and effective Hamiltonian  $\hat{H}_{\text{eff}} = \hat{H}_0 - i\hbar c^\dagger c/2$ . Starting from the time  $t_0$ , a random number  $r$  between 0 and 1 is generated with uniform probability, and we solve the effective Schrödinger equation

$$\frac{d}{dt} |\psi(t)\rangle = -\frac{i}{\hbar} \hat{H}_{\text{eff}} |\psi(t)\rangle \quad (8)$$

until the time moment  $t_j$  such that  $\langle \psi(t_j) | \psi(t_j) \rangle = r$ . At this time moment, a photon is detected and the jump operator is applied to the state of the system, which is subsequently normalised:

$$|\psi(t_j)\rangle \rightarrow \frac{c |\psi(t_j)\rangle}{\sqrt{\langle \psi(t_j) | c^\dagger c | \psi(t_j) \rangle}}. \quad (9)$$

Finally, a new random number is generated and the procedure is iterated setting  $t_j$  as a new starting time. This technique allows to simulate a single quantum trajectory, thus modelling result of a single experimental run.

- 
- [1] Lewenstein, M., Sanpera, A. & Ahufinger, V. *Ultracold atoms in optical lattices. Simulating quantum many-body systems.* (Oxford: Oxford University Press. xiv, 479 p., 2012).
- [2] Diehl, S. *et al.* Quantum States and Phases in Driven Open Quantum Systems with Cold Atoms. *Nature Phys.*

- 4, 878–883 (2008).
- [3] Haroche, S. & Raimond, J.-M. *Exploring the Quantum: Atoms, Cavities, and Photons* (Oxford University Press, 2006).
- [4] Mekhov, I. B., Maschler, C. & Ritsch, H. Cavity-Enhanced Light Scattering in Optical Lattices to Probe

- Atomic Quantum Statistics. *Phys. Rev. Lett.* **98**, 1–4 (2007).
- [5] Mekhov, I. B., Maschler, C. & Ritsch, H. Probing quantum phases of ultracold atoms in optical lattices by transmission spectra in cavity QED. *Nature Phys.* **3** (2007).
- [6] Roscilde, T. *et al.* Quantum polarization spectroscopy of correlations in attractive fermionic gases. *New J. Phys.* **11**, 055041.
- [7] Rogers, B., Paternostro, M., Sherson, J. F. & De Chiara, G. Characterization of Bose-Hubbard models with quantum nondemolition measurements. *Phys. Rev. A* **90**, 043618 (2014).
- [8] Eckert, K. *et al.* Quantum Non-Demolition Detection of Strongly Correlated Systems. *Nature Phys.* **4**, 50–54 (2008).
- [9] Hauke, P., Sewell, R. J., Mitchell, M. W. & Lewenstein, M. Quantum control of spin correlations in ultracold lattice gases. *Phys. Rev. A* **87**, 021601 (2013).
- [10] Mekhov, I. B. & Ritsch, H. Quantum Nondemolition Measurements and State Preparation in Quantum Gases by Light Detection. *Phys. Rev. Lett.* **102**, 1–4 (2009).
- [11] Baumann, K., Guerlin, C., Brennecke, F. & Esslinger, T. Dicke quantum phase transition with a superfluid gas in an optical cavity. *Nature* **464**, 1301–1306 (2010).
- [12] Wolke, M., Klinner, J., Kessler, H. & Hemmerich, A. Cavity cooling below the recoil limit. *Science* **337**, 85–87 (2012).
- [13] Schmidt, D., Tomczyk, H., Slama, S. & Zimmermann, C. Dynamical Instability of a Bose-Einstein Condensate in an Optical Ring Resonator. *Phys. Rev. Lett.* **112**, 115302 (2014).
- [14] Mekhov, I. B. & Ritsch, H. Quantum optics with ultracold quantum gases: towards the full quantum regime of the light-matter interaction. *J. Phys. B* **45**, 102001 (2012).
- [15] Ritsch, H., Domokos, P., Brennecke, F. & Esslinger, T. Cold atoms in cavity-generated dynamical optical potentials. *Rev. Mod. Phys.* **85**, 553 (2013).
- [16] Landig, R., Brennecke, F., Mottl, R., Donner, T. & Esslinger, T. Measuring the dynamic structure factor of a quantum gas undergoing a structural phase transition arXiv:1503.05565.
- [17] Kozłowski, W., Caballero-Benitez, S. F. & Mekhov, I. B. Probing Matter-Field and Atom-Number Correlations in Optical Lattices by Global Nondestructive Addressing arXiv:1411.7567v1.
- [18] Meineke, J. *et al.* Interferometric measurement of local spin fluctuations in a quantum gas. *Nature Phys.* **8**, 455–459 (2012).
- [19] Sanner, C. *et al.* Correlations and Pair Formation in a Repulsively Interacting Fermi Gas. *Phys. Rev. Lett.* **108**, 240404 (2012).
- [20] Wiseman, H. M. & Milburn, G. J. *Quantum Measurement and Control* (Cambridge University Press, 2010).
- [21] Pichler, H., Daley, A. & Zoller, P. Nonequilibrium dynamics of bosonic atoms in optical lattices: Decoherence of many-body states due to spontaneous emission. *Phys. Rev. A* **82**, 063605 (2010).
- [22] Elliott, T. J., Kozłowski, W., Caballero Benitez, S. F. & Mekhov, I. B. Multipartite Entangled Spatial Modes of Ultracold Atoms Generated and Controlled by Quantum Measurement. *Phys. Rev. Lett.* **114**, 113604 (2015).
- [23] Mekhov, I. B. & Ritsch, H. Quantum Optics with Quantum Gases. *Laser Phys.* **19**, 610 (2009).
- [24] Mekhov, I. B. & Ritsch, H. Quantum Optical Measurements in Ultracold Gases: Macroscopic Bose Einstein Condensates. *Laser Phys.* **20**, 694 (2010).
- [25] Mekhov, I. B. & Ritsch, H. Atom State Evolution and Collapse in Ultracold Gases during Light Scattering into a Cavity. *Laser Phys.* **21**, 1486 (2011).
- [26] Facchi, P. & Pascazio, S. Quantum Zeno dynamics: mathematical and physical aspects. *J. Phys. A Math. Theor.* **41**, 52 (2009).
- [27] Schäfer, F. *et al.* Experimental realization of quantum Zeno dynamics. *Nature Comm.* **5**, 3194 (2014).
- [28] Signoles, A. *et al.* Confined quantum Zeno dynamics of a watched atomic arrow. *Nature Phys.* **5**, 715–719 (2014).
- [29] Pedersen, M. K., Sorensen, J. J. W. H., Tichy, M. C. & Sherson, J. F. Many-body state engineering using measurements and fixed unitary dynamics. *New J. Phys.* **16**, 113038 (2014).
- [30] Ivanov, D. & Ivanova, T. Feedback-enhanced self-organization of atoms in an optical cavity. *JETP Letters* **100**, 481–485 (2014).
- [31] Fröwis, F. & Dür, W. Measures of macroscopicity for quantum spin systems. *New J. Phys.* **14**, 093039 (2012).
- [32] Mekhov, I. B. & Ritsch, H. Quantum optics with quantum gases: Controlled state reduction by designed light scattering. *Phys. Rev. A* **80**, 1–15 (2009).
- [33] Lee, M. D. & Ruostekoski, J. Classical stochastic measurement trajectories: Bosonic atomic gases in an optical cavity and quantum measurement backaction. *Phys. Rev. A* **90**, 023628 (2014).
- [34] Corney, J. F. & Milburn, G. J. Homodyne measurements on a Bose-Einstein condensate. *Phys. Rev. A* **58**, 2399–2406 (1998).
- [35] Julia-Diaz, B., Torrontegui, E., Martorell, J., Muga, J. G. & Polls, A. Fast generation of spin-squeezed states in bosonic Josephson junctions. *Phys. Rev. A* **86**, 063623 (2012).
- [36] Ruostekoski, J. & Walls, D. Nondestructive optical measurement of relative phase between two Bose-Einstein condensates. *Phys. Rev. A* **56**, 2996–3006 (1997).
- [37] Kaszlikowski, D., Sen(De), A., Sen, U., Vedral, V. & Winter, A. Quantum Correlation without Classical Correlations. *Phys. Rev. Lett.* **101**, 070502 (2008).
- [38] Winkler, K. *et al.* Repulsively bound atom pairs in an optical lattice. *Nature* **441**, 853–856 (2006).
- [39] Stannigel, K. *et al.* Constrained Dynamics via the Zeno Effect in Quantum Simulation: Implementing Non-Abelian Lattice Gauge Theories with Cold Atoms. *Phys. Rev. Lett.* **112**, 120406 (2014).
- [40] Erez, N., Gordon, G., Nest, M. & Kurizki, G. Repulsively bound atom pairs in an optical lattice. *Nature* **452**, 724 (2008).
- [41] Miyake, H. *et al.* Bragg Scattering as a Probe of Atomic Wave Functions and Quantum Phase Transitions in Optical Lattices. *Phys. Rev. Lett.* **107**, 175302 (2011).
- [42] Weitenberg, C. *et al.* Single-spin addressing in an atomic Mott insulator. *Nature* **471**, 319–324 (2011).
- [43] Weitenberg, C. *et al.* Coherent Light Scattering from a Two-Dimensional Mott Insulator. *Phys. Rev. Lett.* **106**, 2–5 (2011).
- [44] Bakr, W. S., Gillen, J. I., Peng, A., Folling, S. & Greiner, M. A quantum gas microscope for detecting single atoms in a Hubbard-regime optical lattice. *Nature* **462**, 74–77 (2009).
- [45] Patil, Y., Chakram, S. & Vengalattore, M. Quantum



- Control by Imaging: The Zeno effect in an ultracold lattice gas. arXiv:1411.2678.
- [46] Mekhov, I. B. Quantum non-demolition detection of polar molecule complexes: dimers, trimers, tetramers. *Laser Phys.* **23**, 015501 (2013).
- [47] Blatt, R. & Roos, C. F. Quantum simulations with trapped ions. *Nature Phys.* **8**, 277–284 (2012).
- [48] Hartmann, M., Brandao, F. & Plenio, M. B. Strongly interacting polaritons in coupled arrays of cavities. *Nature Phys.* **2**, 849–855 (2006).
- [49] Trauzettel, B., Bulaev, D. V., Loss, D. & Burkards, G. Spin qubits in graphene quantum dots. *Nature Phys.* **3**, 192–196 (2007).
- [50] Fink, J. M. *et al.* Dressed Collective Qubit States and the Tavis-Cummings Model in Circuit QED. *Phys. Rev. Lett.* **103**, 083601 (2009).